Journal of Building Engineering 66 (2023) 105897

Contents lists available at ScienceDirect

Journal of Building Engineering

journal homepage: www.elsevier.com/locate/jobe

Post-tensioned rocking dissipative timber wall systems: Numerical prediction

Valentina Tomei [a,*], Maria Zucconi [b], Barbara Ferracuti [b]

[a] Department of Civil and Mechanical Engineering, University of Cassino and Southern Lazio, via G. Di Biasio 43, 03043, Cassino, Italy
[b] Department of Civil and Industrial Engineering, Niccolò Cusano University, Via Don Gnocchi 3, 00166, Rome, Italy

ARTICLE INFO

Keywords:
Post-tensioned timber walls
Dissipative dampers
Rocking walls
Numerical modeling

ABSTRACT

Low-damage post-tensioned technologies were born with the aim to obtain structural solutions able to guarantee, in case of seismic events, not only the safeguarding of human life, but also the rapid re-use of the buildings without permanent damage. In this context, structural systems based on rocking dissipative timber walls have been introduced, in which rocking behavior is entrusted to post-tensioned bars, and the dissipative contribution is provided by steel dampers, easily replaceable after an intense seismic event. The paper presents a nonlinear numerical model to predict the response of different configurations of Post-Tensioned (PT)-timber wall systems, particularly useful to support the design phase. More in detail, the geometrical non-linearity due to the rocking behavior of the system and material non-linearities that characterize the dampers are taken explicitly into account. The proposed numerical modelling strategy has been validated on different experimental literature tests performed by non-linear static analyses on both single and double wall systems equipped with different damper configurations. The comparison between numerical and experimental results is performed to demonstrate the effectiveness of the proposed model in predicting the behavior of post-tensioned walls subjected to cyclic loads. Further, parametric analyses have been developed in order to investigate the effect of different parameters, such as wall dimensions, initial post-tensioned force in the bars, number of axial and shear dampers, on the global behaviour of post-tensioned timber systems.

1. Introduction

The development of the new technologies in the last two decades has been accompanied by a great evolution of timber building systems against seismic actions [1–5]. The most diffuse timber buildings are made of Cross Laminated Timber (CLT) walls connected to each other and to the foundation by steel connectors, i.e. angle-brackets, hold-downs, nails, and screws. Since the timber panels cannot provide a ductile behaviour, they should work in the elastic fields also during a seismic event, meaning that the energy dissipation is mainly entrusted to steel connectors, which, therefore, can be severely damaged after a seismic event [6–8]. In this system, both internal and external timber walls are load bearing elements; this leads to some drawbacks from both structural and functional points of view. From the structural point of view, CLT systems are characterized by a massive structure with excessive use of material, while from the functional point of view, it is not possible to move the internal walls. In this context, low-damage rocking post-tensioned systems [9–11] want to reduce the structural mass by entrusting vertical loads to a light frame structures, and the seismic loads to Post-Tensioned (PT) walls equipped with hysteretic dampers [9,10], thus limiting the amount of necessary material while improving

* Corresponding author.
E-mail address: v.tomei@unicas.it (V. Tomei).

https://doi.org/10.1016/j.jobe.2023.105897
Received 6 August 2022; Received in revised form 11 January 2023; Accepted 13 January 2023
Available online 14 January 2023
2352-7102/© 2023 Elsevier Ltd. All rights reserved.

the structural performance against seismic events. This approach has been conceived in analogy to precast post-tensioned concrete elements developed by Stone et al. [12], and then investigated within a five-story building by Priestley et al. [13]. Low damage timber systems are constituted by rocking dissipative timber walls, equipped with steel dampers, designed to dissipate energy through damage and to be easily replaced after a seismic event. The rocking behaviour is entrusted to Post-Tensioned (PT) bars placed inside ad hoc cavities in the wall, which are fixed at the base and anchored at the top of the wall (Fig. 1a). The steel dampers can be positioned in different parts of the wall and work in different ways. In particular, they can be positioned at the base working predominantly in the axial direction - axial dampers - [14–19], or they can be positioned along the elevation of the timber wall, connecting adjacent timber walls/columns and working predominantly in the transversal direction - shear dampers - [19–23]. The global behaviour of the post-tensioned low damage system results in a typical flag-shape force-displacement (F/Δ) curve (Fig. 1b), in which both the re-centering contribution of the PT-bars and the dissipative contribution of the dampers are easily recognizable. Indeed, the bilinear envelope is mainly governed by the rocking behaviour, controlled by the PT-bars, but also by the envelope of the force/displacement response of the dampers, which affects the stiffness of the two branches. On the other hand, the flag amplitude is mainly governed by the dissipative contribution of the steel dampers.

Different system configurations have been analysed and tested in the last decade, which can be differentiated on the basis of the material employed (Laminated Veneer Lumber LVL or Cross Laminated Timber CLT), single or double wall systems [9,10,24–26], presence or absence of boundary columns [27–29], type of dampers employed [19–22].

Several experimental campaigns have been also performed on PT-wall systems [9,25,26,28–31], on CLT core wall subassemblies [32], but also on whole buildings [33] or multi-story/multi-panel solutions [34–38].

Further, recent contributions are devoted to the comparison between post-tensioned timber systems with traditional ones [39–41], comparisons between LVL and CLT post-tensioned solutions applied on single or multiple stacking rocking segments [42], or to the investigation of partition walls on the seismic response of timber buildings equipped with post-tensioned rocking walls [43]. Another interesting contribution, instead, deals with design strategies: Huang et al. [44] proposed an optimization strategy, based on a genetic algorithm, for the displacement-based design of mass timber rocking walls. As a confirmation of the validity and the growing diffusion of PT-walls systems, different buildings are recently designed and constructed in New Zealand adopting this innovative structural idea. Further, the main step for the design of post-tensioned timber buildings are also introduced in the Australian and New Zealand design guidelines [45].

The previous discussion suggests the importance of developing numerical models able to capture the experimental responses of PT-wall systems, which can be employed to support the design phase. In this context, some numerical models are proposed and validated on experimental results [9,24,29–31,46,47], while other ones are developed to numerically investigate the different behaviour of PT-wall systems and traditional CLT ones [39–42]. In particular, Sarti [30] proposed two different approaches: i) a simplified modelling approach, called “Lamped Plasticity Model”, which consists of a series of rotational springs that concentrate the system’s behaviour at the base of the wall element, able to capture the global behaviour of the system in terms of Force/Drift response and PT-Force/Drift one; ii) a more refined approach, called “Multi Spring Model”, which is able to provide, in addition to global results, also local information on neutral axis depths, thanks to its capacity to reproduce the rocking behaviour of the walls through an ad hoc compression-only multi-spring element. Both models are developed in the OpenSEES framework [48]. More in detail, the “Lamped Plasticity Model” concentrates the re-centering contribution of the PT-bar and the dissipative contribution of dampers in a couple of rotational springs calibrated on the base of an analytical moment-rotational analysis. These two contributions are modelled with a multi-linear elastic constitutive law for the re-centering rotational spring and an elastic-plastic relationship for the dissipative contributions. The walls/columns have been modelled by means of beam-column elements connected to each other among rigid trusses. The numerical results have been compared with the experimental ones [30] in terms of Force/Drift and PT-Force/Drift responses. Similar approaches have been proposed by Iqbal et al. [9] to simulate double wall systems connected along elevation with shear dampers, and another approach very similar to the “Multi Spring Model” has been presented by Ganey [49] in order to simulate both single wall systems without dampers and double wall systems connected with shear dampers [24]. While the previously described

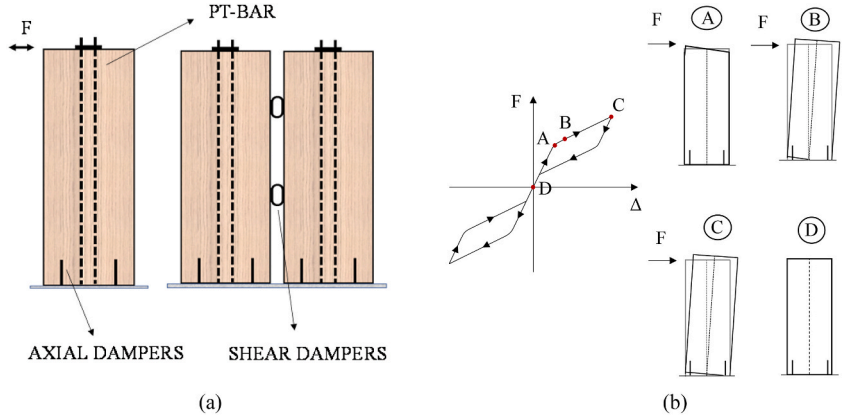


Fig. 1. (a) Typical PT-wall systems; (b) typical flag-shape force/displacement (F/Δ) curve of a PT-system subjected to cycling loading.

numerical models are developed by means of mono-dimensional elements, recently, other approaches propose the use of bidimensional elements, which are able to provide more detailed local information. In this context, Wilson et al. [46] proposed a high-order model that allows to obtain a detailed assessment of local behaviours, such as local stresses distribution throughout the wall and crushing behaviour at the wall toes, which could be employed to calibrate a reduced-order model that guarantees a low computation effort in case of assessment of building responses in time-history analyses. Both models have been developed in the commercial software SAP2000 [50], and validated on the experimental results of Ganey et al. [24] for single wall setups without dampers and double wall systems connected with shear dampers. Then, Chen et al. [51] proposed another numerical model, developed in ABAQUS [52], based on the employ of bidimensional elements in order to simulate the timber panel, validated on the experimental campaign conducted by Chen et al. [26] performed on both single and double wall setups, equipped with axial and/or shear dampers disposed in different configurations. Each of the proposed models described above is able to capture experimental responses, but all of them have been validated on the results of a single experimental campaign. On the other hand, it could be interesting to obtain a numerical model able to reproduce the response of various experimental campaigns. Further, all the described numerical models, have been developed by employing self-made elements or constitutive laws, or these are developed by using non-opensource software; therefore, the proposed strategies are not easily reproducible by the scientific community and/or practitioners. In this context, this paper aims to propose a modelling strategy able to capture the results of several experimental campaigns, assuming a more general validity, by employing an open-source software and components already available, in order to propose a modeling strategy accessible to the scientific community. In particular, the paper presents a nonlinear numerical model, developed in OpenSEES [48], able to account for both geometrical and material non-linearities, and validated on different experimental campaigns. Further, a comparison between numerical and experimental results is proposed in terms of global responses, in particular Force/Drift responses, Post-Tension Force (PT-Force)/Drift curves and Cumulated Dissipative Energy. Then, also some local responses will be shown, highlighting the capacity of the numerical model to provide information that are difficult to obtain (or not available) from an experimental campaign, such as the uplift along the base and elevation, and the Force/Displacement responses of the dampers, which particularly affects the dissipation energy provided by the whole system. Moreover, a parametric study has been introduced in order to investigate the effect of different parameters (wall dimensions, initial post-tensioned force in the bars, number of axial and shear dampers) on the global response of PT-wall systems, in terms of strength, stiffness, re-centering contribution and dissipation capacity.

2. Experimental campaigns

Some of the setups of the experimental campaigns mentioned in the Introduction (section 1) have been taken into account to validate the proposed numerical model, and they are schematically described in Table 1. In particular, they can be distinguished on the base of:

- number and type of timber elements (W: single wall; WW: double wall; CWC: single wall with boundary columns/column-wall-column);
- type of timber (LVL or CLT);
- type and position of dampers (A: axial dampers positioned along the base of the timber wall; S: shear dampers positioned along elevation; AS: both axial and shear dampers);
- number of PT-bars for each wall (n. PT bar/wall).

In order to immediately identify the first three characteristics, the different tests are renamed and reported in Table 1-first column: for example, W_LVL_A indicates a setup characterized by a single wall (W) made of Laminated Veneer Lumber (LVL) and equipped with axial dampers (A), while WW_CLT_AS indicates a setup characterized by a double wall (WW) made of Cross Laminated Timber (CLT) and equipped with both axial (A) and shear (S) dampers, and so on.

Further, detailed information on the selected experimental campaigns, derived from the literature results, are reported in Fig. 2 in terms of geometrical characteristics, material properties and initial PT-Force imposed to the PT-bars for each setup, where: about timber elements, E_L and E_T indicates the elastic moduli of the timber, G_{LT} and G_{LR} indicate the shear moduli of the timber, with subscripts L, T, R that indicate longitudinal, transverse and radial directions, respectively; about PT-bars, E_b is the elastic modulus of the steel, $PT\text{-}F_{in}$ is the initial PT-Force; about axial dampers, $f_{y,A}$ and E_A are the yielding stress and the relevant elastic modulus of the axial damper; about shear dampers, $f_{y,S}$ and E_S are the yielding stress and the relevant elastic modulus of the shear damper.

Table 1
Experimental campaigns selected for validation of the proposed numerical model.

Setup	Experimental Campaigns	System	Dampers	Timber	n. PT bar/wall
W_LVL_A	Sarti et al. [10]	W	A	LVL	2
W_CLT_A	Chen et al. [26]	W	A	CLT	1
CWC_LVL_S	Sarti et al. [28]	CWC	S	LVL	2
WW_CLT_A	Chen et al. [26]	WW	A	CLT	1
WW_CLT_S	Chen et al. [26]	WW	S	CLT	1
WW_LVL_S	Iqbal et al. [9]	WW	S	LVL	2
WW_CLT_AS	Chen et al. [26]	WW	A + S	CLT	1

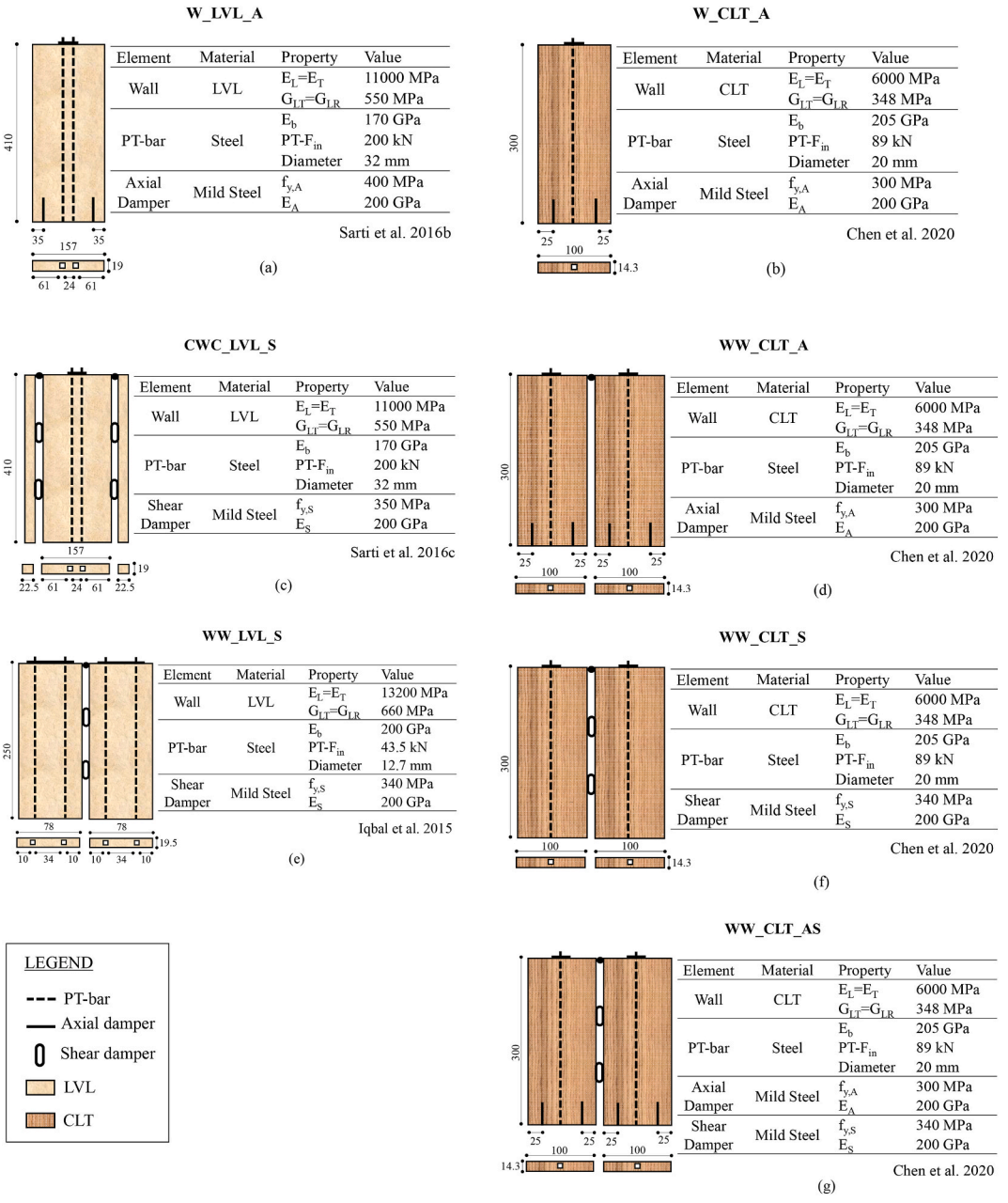


Fig. 2. Setups of the experimental campaigns employed to validate the proposed numerical model.

3. Proposed numerical model

3.1. Description of the proposed numerical nonlinear model

The proposed numerical models have been developed in OpenSEES [53] as a 2D model, which accounts for both geometrical and mechanical non-linearities. The former is related to the rocking behaviour of the walls, while the latter is mainly due to the entering into the plastic field of axial and shear steel dampers, simulated by nonlinear springs able to reproduce their hysteretical response. A schematical description of the numerical models is presented in Fig. 3 for the single wall (SW), column-wall-column (CWC) and double wall (WW) setups, respectively, but the description of the structural elements is the same for all.

Timber elements have been modelled as elastic 2D Quad elements, to which a linear elastic orthotropic stress/strain (σ/ε) law is assigned on the base of the mechanical properties of the timber employed for each setup, described in Fig. 2. The PT-bars have been modelled through two node link elements, characterized by an elastoplastic force-displacement curve with elastic stiffness K (Fig. 3), to which an initial elastic deformation ε_{in} is associated in order to simulate the post-tensioning force provided at the beginning of each

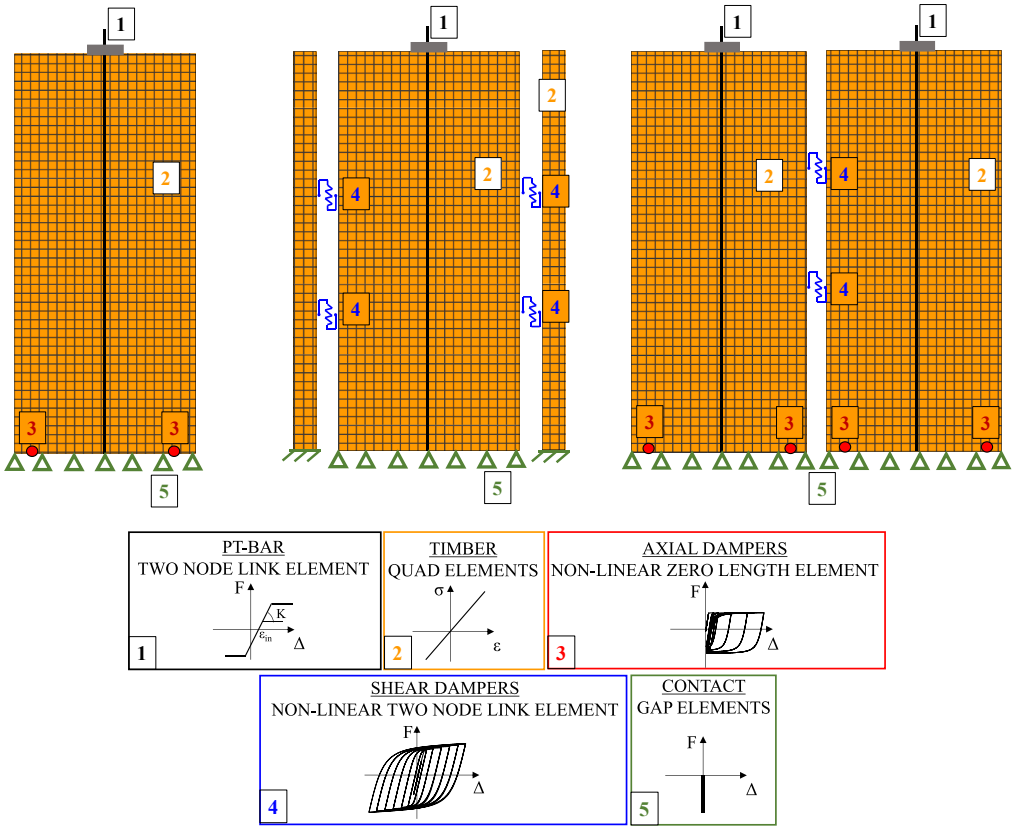


Fig. 3. Numerical meshes of single wall setup, single wall setup with boundary columns and double wall setup.

test. These elements are fixed at the base and connected at the top to the relevant wall. For the modelling of tests provided by axial and/or shear dampers, nonlinear springs simulating their behaviour have been introduced, taking into account the hysteretical behaviour under cyclic loading. The relevant force-displacement laws assigned to the nonlinear springs have been calibrated on the base of the experimental force-displacement response, as will be explained in section 3.2. Moreover, the walls are constrained at the base by means of zero-length elements, which is associated with a no-tension material characterized by an infinite stiffness in compression, in order to simulate a series of unilateral constraints (gap elements), which are able to capture the rocking behaviour of the system. Further, the shear transfer devices have been modelled by imposing equal horizontal displacement (EqualDOF in OpenSEES) to the nodes of adjacent timber walls/columns disposed at the interface between the timber element and the shear transfer device.

All the simulated systems have been subjected to increasing cycling displacements imposed at or close the top of the walls, whose precise loading history and position of application have been chosen in analogy to that employed during the experimental campaigns.

Table 2
Parameters defining the behaviour of axial and shear dampers.

Constitutive law	Parameters	AXIAL DAMPERS		SHEAR DAMPERS	
		W_LVL_A	W_CLT_A WW_CLT_AS	CWC_LVL_S	WW_LVL_S WW_CLT_S WW_CLT_AS
STEEL 02	F_y (kN)	65	42.5	–	23
	E (MPa)	85000	43000	–	10000
	b	0.01	0.02	–	0.01
	R0	40	50	–	18
	c_{R1}	0.955	0.955	–	0.955
	c_{R2}	0.15	0.2	–	1
RAMBERG-OSGOOD	F_y (kN)	–	–	10	–
	E (MPa)	–	–	7500	–
	a	–	–	0.06	–
	n	–	–	4	–

About the computational effort, it is mainly related to the refinement of the mesh of bidimensional elements; since the timber elements work predominantly in the elastic field, it is possible to assume a mesh not too dense in order to minimize the computational effort. In this work, each panel is discretized by quadrangular mesh with dimensions of 10 cm for side; by performing non-linear static analyses, the required time is about 8 min for the single wall with dampers and 12 min for the double wall setup with dampers; further developments will concern dynamic analyses. The analyses have been performed with a processor with the following characteristics: Intel(R) Core(TM) i7-7700HQ CPU @ 2.80 GHz, 2808 Mhz, 4 core, 8 logical processors.

3.2. Hysteretical models for dissipation devices

The nonlinear laws adopted for the axial and shear dampers have been calibrated on the basis of preliminary shear and axial experimental tests performed on the single components by minimizing the differences in terms of Cumulated Dissipated Energy (CDE), strength and stiffness between the numerical response and the experimental one. The adopted numerical law is the OpenSEES "Steel 02" law for both axial and shear dampers, which corresponds to the Giuffré-Menegotto-Pinto Model with Isotropic Strain Hardening [54], except for the shear dampers employed for the WW_LVL_S [9], which behaviour has been modelled through the OpenSEES Ramberg Osgood Steel law [55], which better minimize the differences between the experimental and numerical response, in this specific case. Table 2 shows the values assigned to the parameters of both constitutive laws, for all the dampers. In particular, the "Steel 02" law is characterized by: F_y, the yield strength; E, initial elastic tangent stiffness; b, hardening ratio; $R0$, $c_{R1}$and c_{R2}, which are parameters that control the transition from elastic to plastic branches [54]. The "Ramberg Osgood Steel" law is instead described by: F_y; E; a, which define the yield offset; n, which controls both the transition from elastic to plastic branches and the hardening of the material [55].

The comparisons between the experimental cyclic behaviour of dampers and the calibrated numerical responses, in terms of force-displacement curves, are reported for all setups. In particular, among the selected experimental tests (Table 1), the axial dampers were adopted only by Sarti et al. [10] and by Chen et al. [16]. Fig. 4a and b shows the comparison between the experimental and numerical behaviour of axial dampers employed for the W_LVL_A and W (WW)_CLT_A(AS) setups, respectively.

For the shear dampers, Fig. 5a shows the comparison for the shear dampers of the CWC_LVL_S setup by Sarti et al. [15], the only ones modelled with the Ramberg Osgood Steel law, which better captures the offset between successive cycles, while Fig. 5b shows the comparison for the WW_LVL_S [9], WW_CLT_S [16], WW_CLT_AS [16], which use the same type of UFP-shape dampers. The comparisons show a good agreement in terms of backbone curve, and so in terms of strength and stiffness, while some local differences can be found in the unloading branches, mainly due to some shifts in terms of displacement at zero-force in the experimental response of axial dampers (Fig. 4b), or to the asymmetric experimental response of shear dampers (Fig. 5a and b). In order to evaluate the differences in terms of energy dissipation, the CDEs (Cumulative Dissipated Energy) are evaluated for both numerical and experimental results and reported in Fig. 6, showing a perfect match for low cycle number and a good match for high cycle number.

4. Validation of the proposed numerical model

4.1. Global results

Results in terms of Force/Drift responses and PT-Force/Drift curves are reported in Fig. 7 for single wall (W) and column-wall-column (CWC) setups, in Figs. 8 and 9 for double-wall setups (WW). All the Force/Drift curves show a well-defined bilinear curve, in which the transition point between the first branch and the second one corresponds to the drift to which at least one PT-bar is subjected to an increment of tension. Further, the dissipative contribution provided by the hysteretic dampers is evident considering the cyclic response. About PT-Force/Drift curves, in all cases, it is evident an increment of PT-Force moving from the position of zero drift towards a drift larger than zero in absolute value, strictly related to the rocking behaviour of the walls, which causes an elongation of the PT-bars. Discussing in details the results of the single setups, the numerical Force/Drift response of the W_LVL_A setup [10], which is characterized by a single wall equipped with two PT-bar and two couples of axial dampers, shows a good agreement with the experimental curve (Fig. 7a) in terms of initial stiffness, strength and cyclic behaviour. About the comparison in terms of

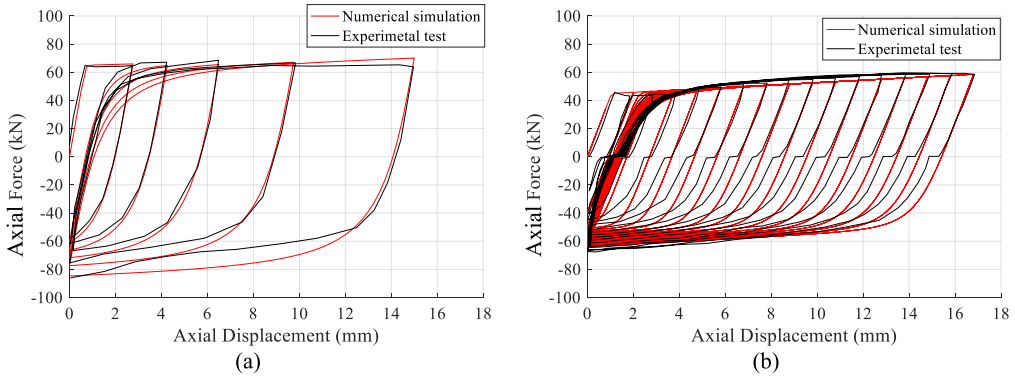


Fig. 4. Calibration of axial dampers: (a) W_LVL_A; (b) W_CLT_A and WW_CLT_AS.

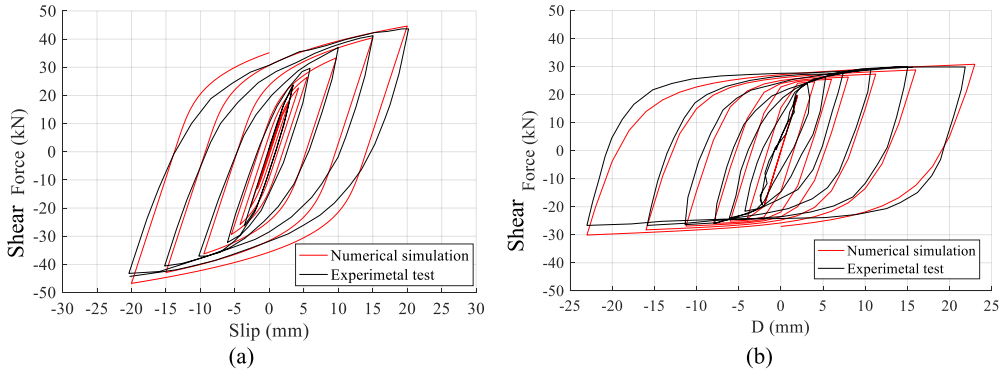


Fig. 5. Calibration of shear dampers: (a) CWC_LVL_S; (b) WW_LVL_S, WW_CLT_S, WW_CLT_AS.

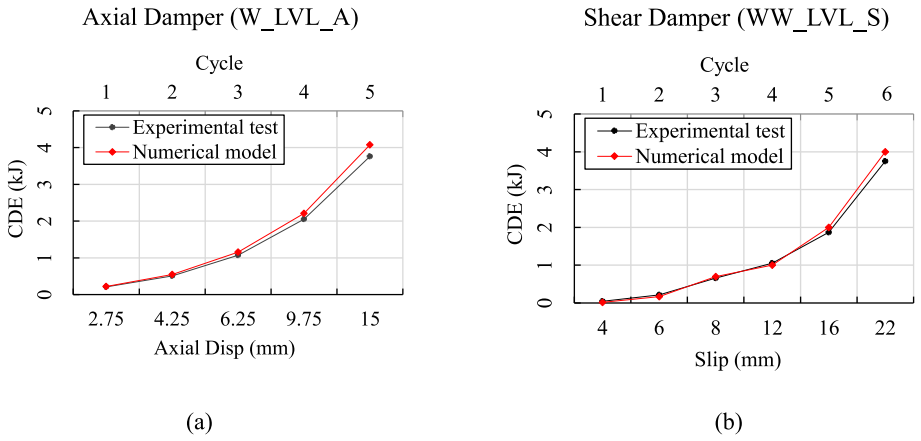


Fig. 6. Comparison of CDEs between experimental and numerical behaviour of the dampers: (a) axial damper employed in the setup W_LVL_A; (b) shear dampers employed in the setup WW_LVL_S.

PT-Force/Drift curves (Fig. 7b), the numerical model well captures the variation of PT-Force, showing a slight difference in the response of the PT-bar positioned to a greater distance from the wall corner subjected to uplifts during the rocking, which is also subjected to a lower variation of PT-Force than the closest the PT-bar.

Concerning the W_CLT_A setup [12], characterized by a similar setup to the previous one in terms of structural components, the wall in CLT is more deformable with respect to the LVL one and the applied initial PT-Force is about a quarter than the one applied in W_LVL_A. The response of W_CLT_A is characterized by a Force/Drift curve with values of drift different from zero at zero force due to the evidence that the dissipation energy provided by the dampers is more pronounced than the recentring contribution provided by the PT-bar. For the same reason, the envelope moves away from the classic bilinear curve since the backbone curve is strongly affected by the contribution of dampers also in terms of strength. By observing the PT-Force/Drift curve, this trend further shows the poor re-centering of the wall, since as the number of cycles increases, also the PT-Force at zero drift increases. This behaviour is well-captured by the numerical model, also if some difference is present in terms of PT-Force variation (the difference reaches the 20% for the maximum imposed drift of 2.5%).

About the CWC_LVL_S setup, the comparison of experimental and numerical Force/Drift responses (Fig. 7b) shows a good agreement in terms of backbone curve, except for a slight difference in stiffness on the second branch. A greater difference is evident in terms of dissipated energy due to considerable frictional effects provided by the different elements assembled in the experimental setup, which have been neglected in the numerical model.

Shifting the discussion to the double wall (WW) setups, Fig. 8a shows a good agreement between the numerical and experimental Force/Drift curve for the WW_CLT_A setup, while the results in term PT-Force/Drift curve for the two PT-bar of the two walls are reported only for the numerical response since the experimental one is not available in the literature. It is evident that when shear dampers are missing, both the two PT-bar show numerically the same variation of PT-Force.

Focusing on the WW_CLT_S setup, similar to the previous one but equipped with shear dampers instead of axial ones, the numerical model overestimates the stiffness of the first and second branches of the Force/Drift curve (Fig. 8c). About PT-bar/Drift curves, only the numerical results are reported, which show, by observing the single PT-bar belonging to one of the two walls, an asymmetrical behaviour in terms of PT-Force variation for positive and negative branches: this asymmetry is due to an incomplete transfer of uplifts

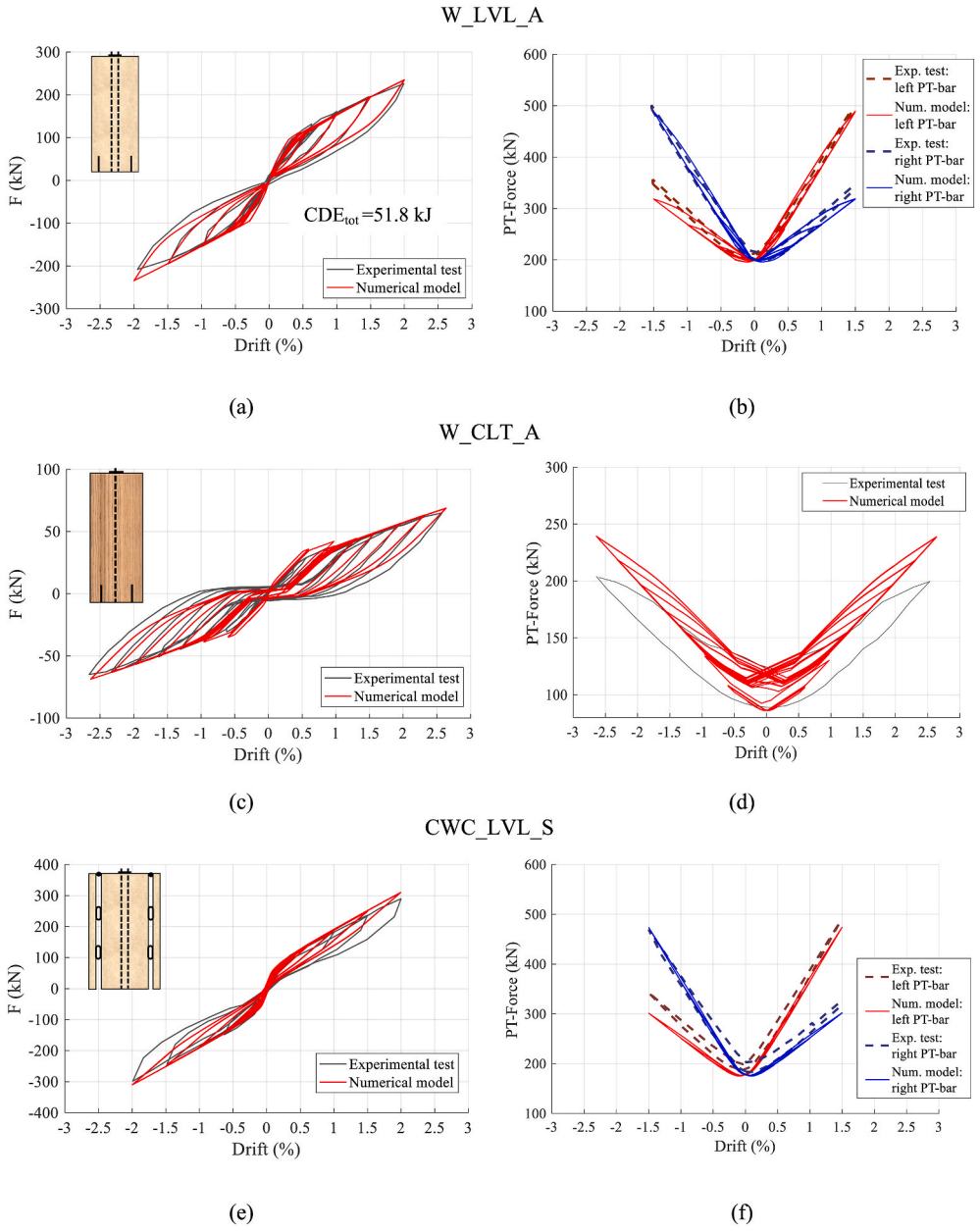


Fig. 7. W_LVL_A: (a) Force/Drift response and (b) PT-Force/Drift curve; W_CLT_A: (c) Force/Drift response and (c) PT-Force/Drift curve; CWC_LVL_S: (e) Force/Drift response and (f) PT-Force/Drift curve.

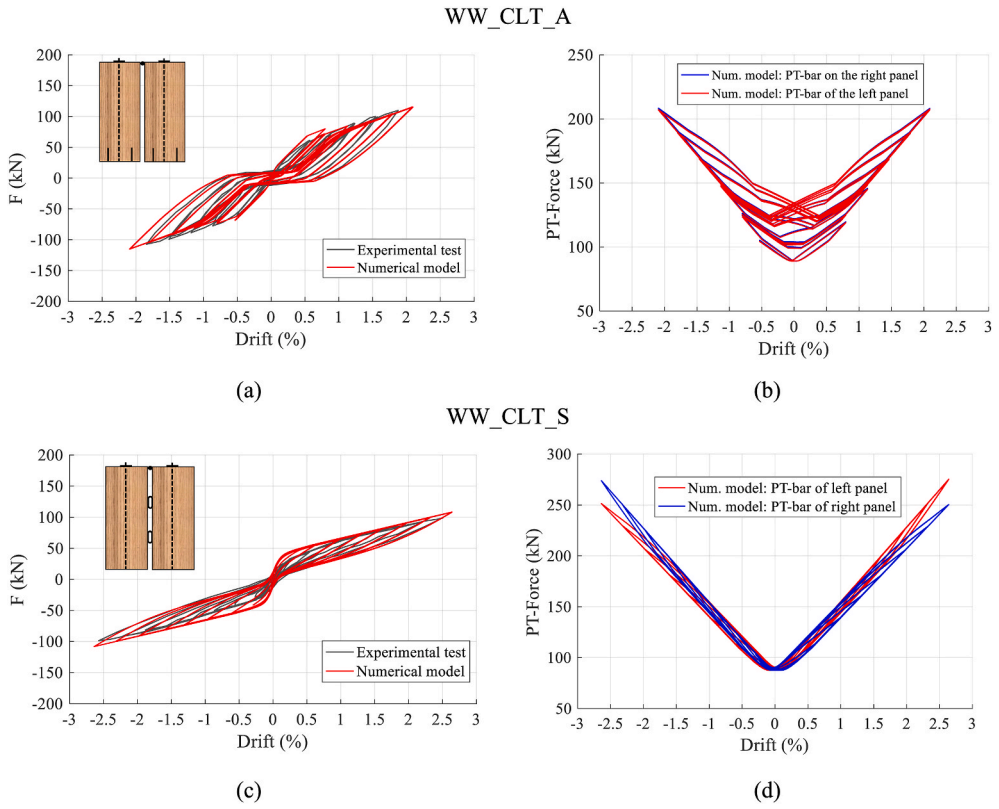


Fig. 8. WW_CLT_A: (a) Force/Drift response and (b) PT-Force/Drift curve; CWC_CLT_S:(c) Force/Drift response and (d) PT-Force/Drift curve.

between the connected sides of the walls, due to the presence of shear dampers. In any case, the behaviour is the same for the two PT-bars. A similar trend is shown by the experimental results in terms of PT-Force variation of the WW_LVL_S setup (Fig. 9b), also if characterized by two PT-bars for each wall. The asymmetry is less evident in this case because of a greater re-centering contribution (PT-Force 4x43,5 kN). The Force/Drift response shows a good agreement in terms of backbone curve, especially for negative drifts, while in general, the energy dissipation is well captured. The WW_CLT_AS setup is very similar to the WW_CLT_A and WW_CLT_S ones; the only difference is that it is equipped with both axial and shear dampers. So, the same considerations made for WW_CLT_A and WW_CLT_S setups are also valid and evident in this case, and the results show a good agreement between experimental and numerical responses (Fig. 9c and d).

Fig. 10 shows the numerical/experimental comparisons in terms of CDE - evaluated in reference to the first cycle of each peak value of drift - for some of the configurations equipped with axial dampers (W_LVL_A in Fig. 10a) and both axial and shear dampers (WW_CLT_AS in Fig. 10b); a very good matching can be found, with differences that reach at maximum 6% and 13% for W_LVL_A and WW_CLT_AS, respectively.

Since the energy dissipation is strictly related to the hysteretic contribution of the dampers, it is expected that the values of the CDE_{tot} evaluated on the global Force/Total Displacement response are equivalent to $CDE_{tot,dam}$, the dampers Cumulative Dissipated Energy. The latter is numerically evaluated by summing the energy dissipated of the single axial dampers computed on the damper Force/Displacement response, considering the effective vertical displacements to which the dampers are subjected during the simulated loading protocol of the entire wall. Confirming this, at title of example, the CDE has been evaluated on the global Force/Total Displacement curve (Fig. 7a) of the W_LVL_A setup and, as will be shown in the following section, on the Force/Displacement response of the four axial dampers, showing the same result of 51.8 kJ.

In this context, it is interesting to evaluate the numerical Dissipated Energy for the first cycle of the *i-th* drift (DE_i), where the analysed drifts are 0.5%, 1%, 1.5% and 2% (Table 3). From Table 3a it emerges that the setups which provide the greatest DE_i are W_LVL_A, CWC_LVL_S and WW_CLT_AS, while W_CLT_A shows the lowest value of DE. The comparison between W_LVL_A and W_CLT_A is interesting, in that, despite being characterized by a similar configuration of dampers, the first has a $DE_{2\%}$ four times larger than the second one. This is mainly due to the axial dampers employed for W_LVL_A setup, characterized by a greater strength than W_CLT_A setup (Fig. 4a and b), which also leads to a greater dissipative capacity. CWC_LVL_S and WW_CLT_AS are characterized by similar values of $DE_{2\%}$, being equipped with the same number of dampers, also if the first one is characterized by shear dampers and the second one by both shear and axial dampers. Also, the WW_CLT_S and WW_LVL_S setups present similar values of $DE_{2\%}$, since they are equipped with the same number of shear dampers that work similarly. Further, it is interesting to note that by adding the $DE_{2\%}$ of the WW_CLT_A and WW_CLT_S setups, the values of $DE_{2\%}$ of WW_CLT_AS are obtained, having the first two setups the same number and

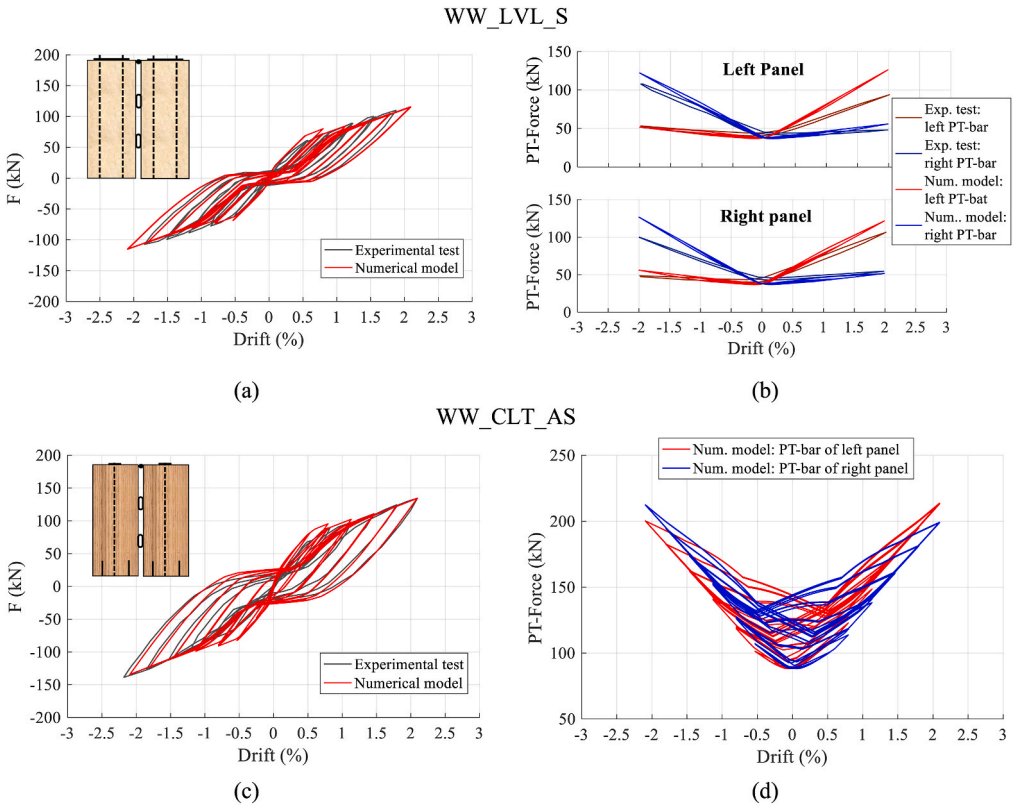


Fig. 9. WW_LVL_S: (a) Force/Drift response and (b) PT-Force/Drift curve; CWC_CLT_AS: (c) Force/Drift response and (d) PT-Force/Drift curve.

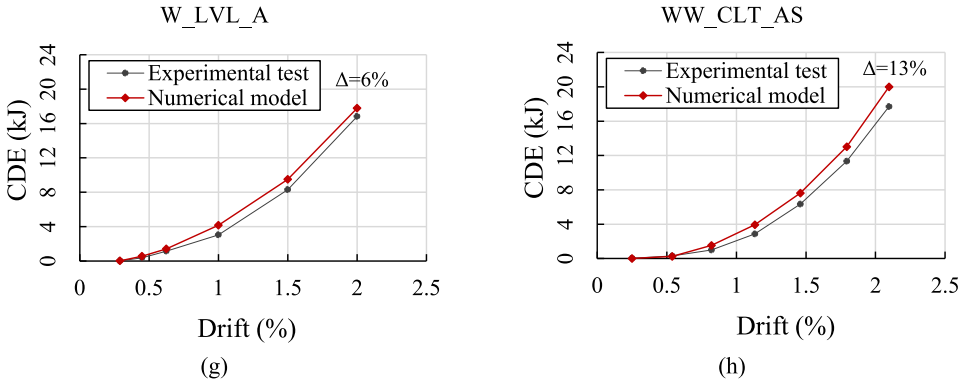


Fig. 10. Cumulated dissipate energy: (a) W_LVL_S; (b) WW_CLT_AS.

type of dampers of the third one. Table 3b shows the ratio between the DE_i of the *i-th* drift and the $DE_{2\%}$, showing that for a drift of 0.5%, the percentage of dissipated energy is in the range 3–12%, while varies between 26 and 40% for the 1% of drift, and changes from 46 to 76% for the 1.5% of drift.

4.2. Local results

A numerical model able to capture the experimental responses allows to obtain also information on local behaviours difficult to get from the experimental point of view, or that simply have not been experimentally analysed. In this context, it could be interesting to plot the uplifts along the base of a transversal cross-section of the wall(s) recorded at a different level of drift, reported in Fig. 11 for different setups (at 20 cm from the base): W_LVL_A (Fig. 11a), CWC_LVL_S(Fig. 11b), WW_CLT_A and WW_CLT_AS (Fig. 11c), WW_LVL_S (Fig. 11d). In all cases, the uplifts show an almost linear trend along the base for each level of drift. Further, by observing the positions of the PT-bars reported in Fig. 11 with thick lines, it is simply to understand that these are subjected to elongation to accommodate the rocking behaviour of the system: this causes the variation of PT-Force observed in section 4.1 in terms of global

Table 3
Values of Dissipated Energy DE_i provided by the first cycle of the i-th drift peak (numerical response).

(a)				
DE_i [kJ]				
Drift				
Setup	0.5%	1%	1.5%	2%
W_LVL_A	0.53	2.75	5.33	8.30
W_CLT_A	0.05	0.58	1.27	1.93
CWC_LVL_S	0.47	1.69	3.85	6.62
WW_CLT_A	0.02	1.14	1.89	4.09
WW_CLT_S	0.34	1.01	2.14	2.84
WW_LVL_S	0.07	1.22	2.29	3.15
WW_CLT_AS	0.24	2.41	3.68	6.93
(b)				
$DE_i/DE_{2\%}$				
Drift				
Setup	0.5%	1%	1.5%	2%
W_LVL_A	0.06	0.33	0.64	1
W_CLT_A	0.03	0.30	0.66	1
CWC_LVL_S	0.07	0.26	0.58	1
WW_CLT_A	0.01	0.28	0.46	1
WW_CLT_S	0.12	0.35	0.75	1
WW_LVL_S	0.02	0.39	0.73	1
WW_CLT_AS	0.03	0.35	0.53	1

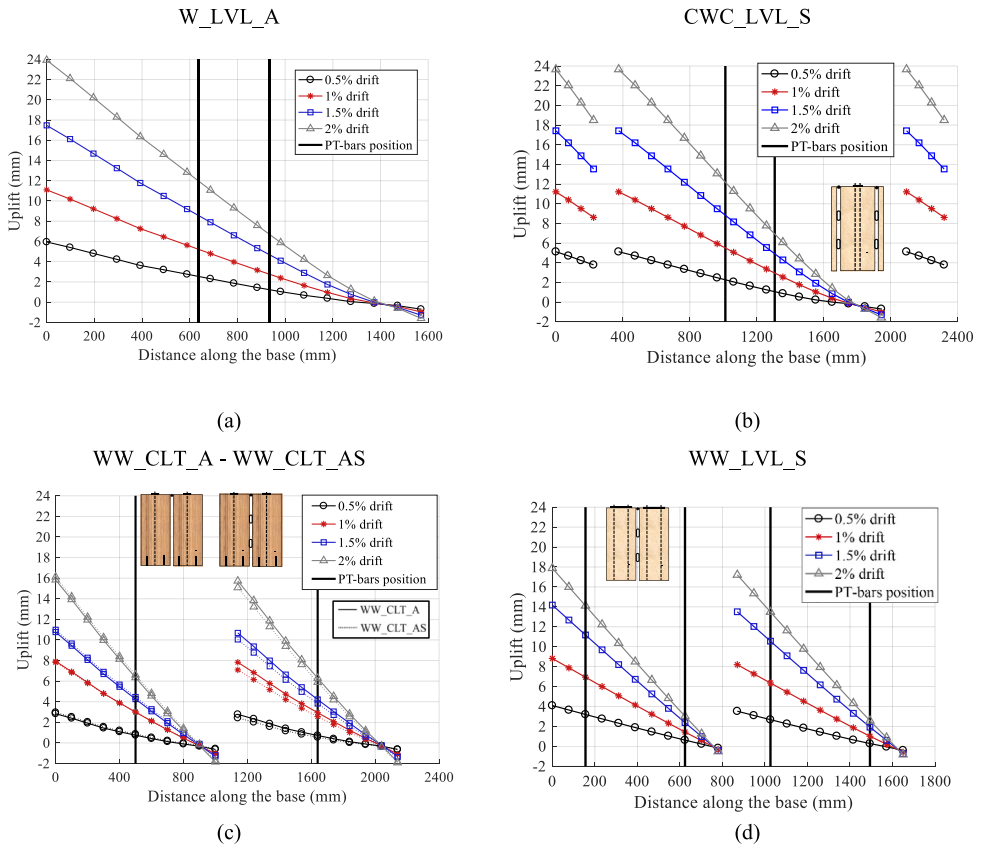


Fig. 11. Uplifts along the base evaluated at 20 cm of elevation from the base.

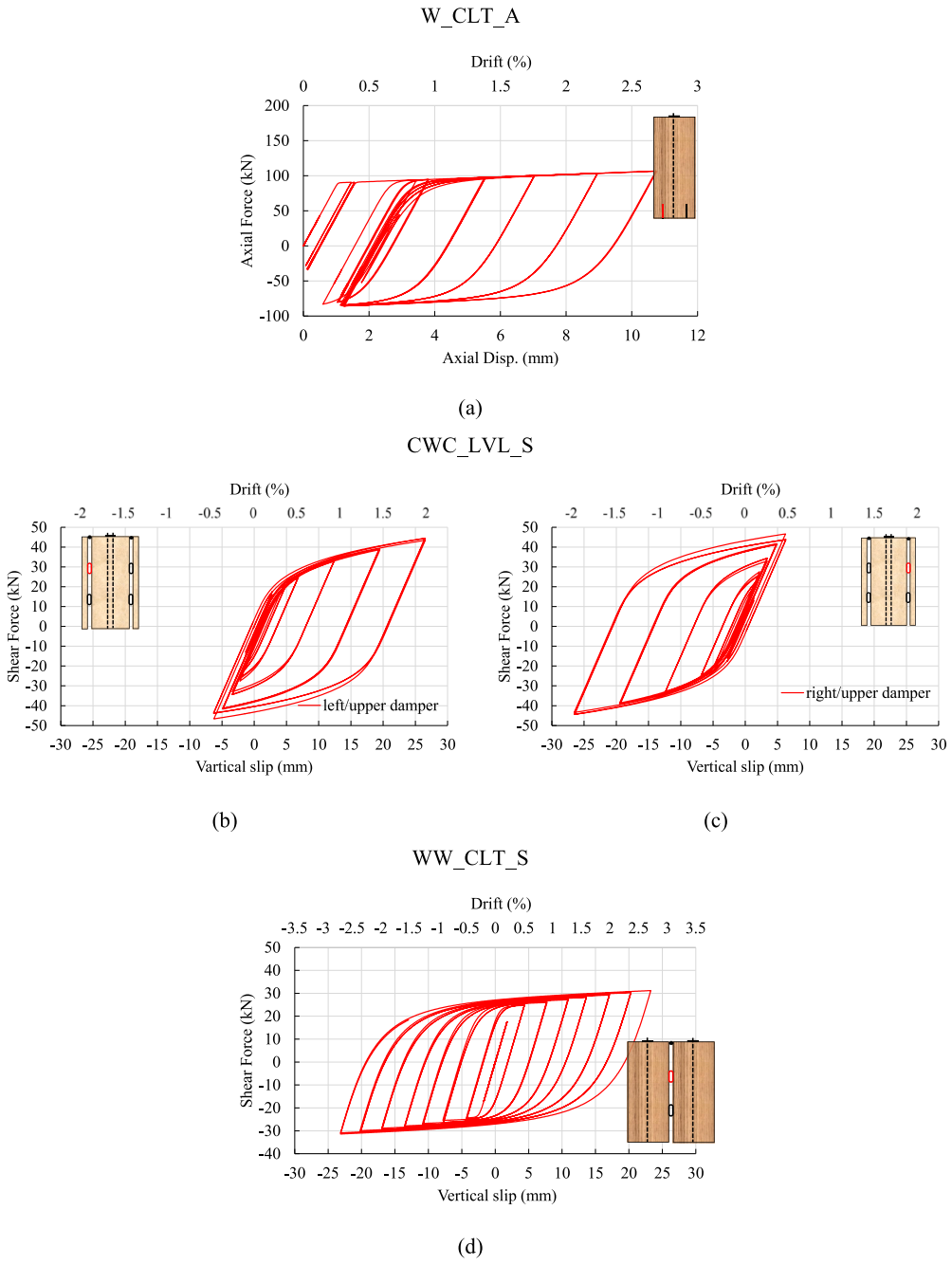


Fig. 12. Force/Displacement response of dampers: (a) axial dampers of W_CLT_A setup; (b) shear damper connecting the left column to the wall and (c) shear damper connecting the wall to the right column of the CWC_LVL_S setup; (d) shear damper of the WW_CLT_S setup.

results. Moreover, by considering setups equipped with more than one PT-bar per wall (Fig. 11a, b and d), the variation in elongation of the PT-bar close to the wall corner that is uplift is the highest one, meaning that it is subjected to a greater PT-Force variation, as also evident for the results in terms of PT-Force/Drift shown in Fig. 7b and f, and in Fig. 9b. Focusing on double wall setups (Fig. 11c and d), observing the uplift of the two walls versus the drift evaluated on the left wall, the setups without shear dampers show equal uplifts of the two walls at the same drift level (Fig. 11c – continuous line), while they slightly differ when shear dampers are provided (Fig. 11c – dot line). It happens because the shear dampers affect the drift transfer from one wall to the other one, which is therefore not identical on the two walls. The drift also influences the base uplifts and, consequently, the PT-Force. Therefore, the drift changes lead to differences in the two walls' PT-Force variation, as evident from the PT-Force/Drift curve in section 4.1 (Figs. 8d and 9b and d).

Further interesting results deal with the dampers' numerical force/displacement response since they provide the dissipation energy

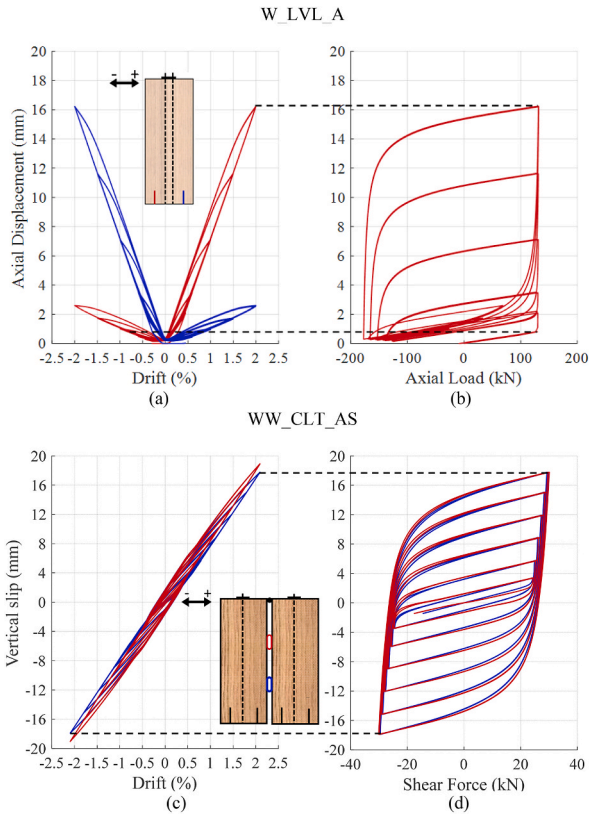


Fig. 13. W_LVL_A: (a) Numerical axial damper responses vs drift: (b) Numerical axial displacement vs axial force; WW_CLT_AS: (c) Numerical shear damper responses vs drift: (d) Numerical shear displacement vs shear force.

contribution of the system. It is relevant to highlight as the force/displacement response of the couples of axial dampers (Fig. 12a – W_CLT_A) is exploited predominantly in one direction to accommodate the rocking behaviour of the system, which allows them to work only in traction; on the other hand, shear dampers are designed to work symmetrically in both positive and negative directions, as for the WW_CLT_AS setup (Fig. 12d), since they generally connect two adjacent walls along elevation: in this case, the rocking behaviour leads to exploit the shear dampers in both directions; instead, if shear dampers connect elements characterized by very different base dimensions (Fig. 12b and c – CWC_LVL_S), as when connecting a column with a wall, the uplifts of the column are limited with respect the ones of the wall, leading the exploitation of the shear damper predominantly in one direction, as also evident from Fig. 11b.

Fig. 13a shows the axial displacements of the axial dampers of the W_LVL_A setup as a function of the drift of the panel: this result is interesting in that the dissipative contribution depends on this parameter, strictly related to the geometry of the panels and to the drift to which it is subjected; obviously, the axial displacement provided by each damper is asymmetric with respect the drift, due to the rocking behaviour which causes greater displacements to the dampers close to the panel corner which uplifts. Further, Fig. 13b shows the axial displacements of the dampers, this time in function of the axial force provided, giving information on the cyclic behaviour of the same.

On the other hand, Fig. 13c shows the vertical slip to which the shear dampers of the WW_CLT_AS setup are subjected as a function of the drift: in this case, vertical slips provided by each damper are the same for both positive and negative drift, except for the sign, in that they are located between two walls characterized by the same base dimensions, which have the same rocking behaviour for both positive and negative drifts. Further, the shear damper located in the bottom part of the walls (the blue one in Fig. 13c), is subjected to smaller vertical slips, this difference is due to the deformability of CLT walls. Fig. 13d, in analogy to Fig. 13b, shows the vertical slips of the shear dampers as a function of the shear force provided by the dampers, giving information on the cyclic behaviour of the same.

5. Parametric analyses

In order to investigate the effect of different parameters on the global behavior of post-tensioned timber walls, some parametric analyses have been developed by varying the wall base B, the wall height H, the initial post-tensioned force $PT\text{-}Force_{in}$ of the bars, the timber characteristics in terms of elastic modulus E (that indicates, for simplicity, the value of $E_L = E_T$ defined in section 2) and shear modulus G (that indicates the value of $G_{LT} = G_{LR}$ defined in section 2), the number of Axial Dampers, starting from the base setup W_CLT_A; the effect of the number of Shear Dampers has been investigated, instead, starting from the base setup WW_CLT_S. The

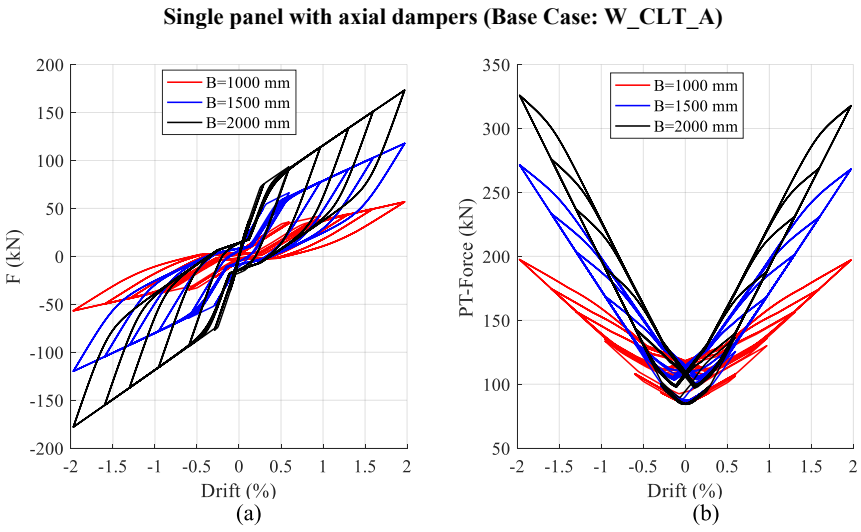


Fig. 14. Effect of the base of the wall B on Force/Drift (a) and PT-Force/Drift curves (b) for single wall setups.

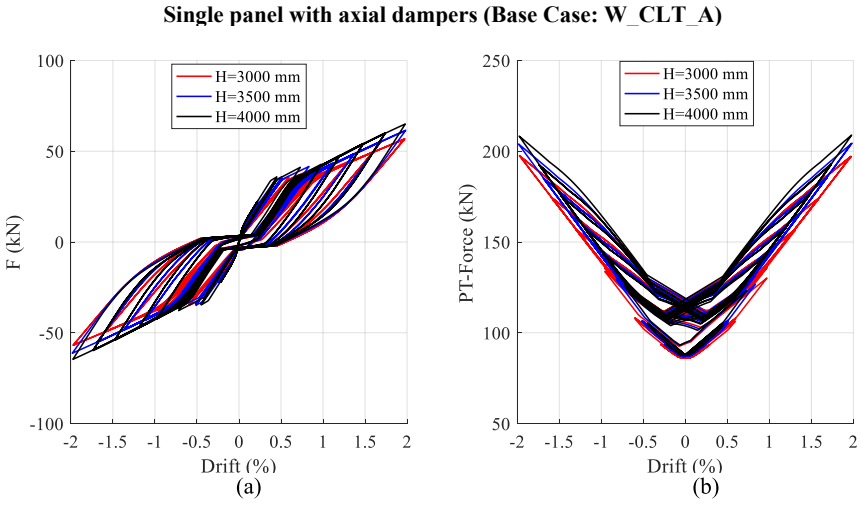


Fig. 15. Effect of the height of the wall H on Force/Drift (a) and PT-Force/Drift curves (b) for single wall setups.

results have been reported in terms of Force/Drift curves and PT-Force/Drift curves from Figs. 14–19, while Table 4 shows the results in terms of the force F^* in correspondence with the transition between the first and second branch in the envelope of the Force/Drift curves, the Force reached at 2% of Drift $F_{2\%}$, Post-tensioned Force variation reached by the bar at 2% of Drift $\Delta PT\text{-}Force_{2\%}$, and the stiffness of the first branch k. Figs. 14a and 15a show that by increasing the dimensions of the wall, there is an increase in terms of strength and stiffness. These effects are more evident when B increases, since the axial dampers are subjected to higher displacement if the distance from the corners remains unchanged from the base setup (W_CLT_A), and therefore provide a more significant contribution in terms of strength and stiffness, but also dissipative capacity. In terms of PT-Force, the variation of the wall base B led to a more significant change (Fig. 14b) with respect to the increase of the wall height H (Fig. 15b). Fig. 16 shows the effect of $PT\text{-}Force_{in}$ in increasing strength, stiffness and, above all, the re-centering capacity of the system, as evident from the flag shape of the Force/Drift curve obtained for an initial PT-Force of 180 kN. Fig. 17 shows the effect of the increase of the elastic modulus E and shear modulus G in increasing strength and stiffness, while no effective difference in terms of dissipative capacity is provided, as shown by the amplitude of the Force/Drift curves. Fig. 18 shows the influence of the number of axial dampers, highlighting their effect in increasing strength, stiffness and, above all, the dissipative capacity of the system; on the other hand, an increasing number of dampers reduces the re-centering capability, evident from the increasing residual drift at zero force. Similarly, Fig. 19 shows the effect of an increasing number of shear dampers in double wall setups, also highlighting their effect in increasing strength and dissipative capacity, while the re-centering capacity of the system is slightly influenced. In this specific case, a reduction of initial stiffness is observed by increasing the number of shear dampers, due to the presence of a smoothed pinching effect that influences the slope of the first branch of the

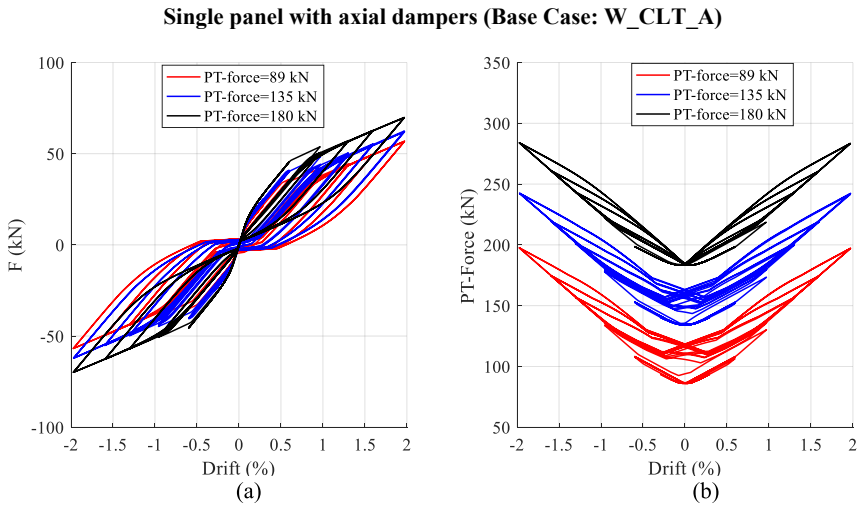


Fig. 16. Effect of the initial PT-Force on Force/Drift (a) and PT-Force/Drift curves (b) for single wall setups.

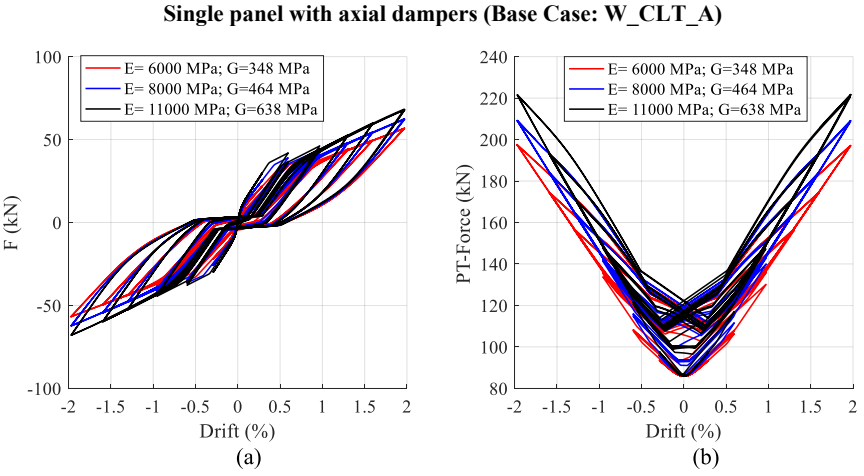


Fig. 17. Effect of the number of timber characteristics (E and G) on Force/Drift (a) and PT-Force/Drift curves (b) for single wall setups.

Force/Drift curve. The same considerations can be deduced by observing the data reported in Table 4, which will be discussed in detail in the following:

- Effect of *B*. As *B* increases, an increase of similar entity (33% and 50%), is observed in terms of F^* and $\Delta PT\text{-}Force_{2\%}$, since it is strictly related to geometrical issues: indeed, for the same value of drift, the uplift of the base of the wall increase linearly with the increase of *B*; a strong increment of $F_{2\%}$ (54% and 68%) and *k* (60% and 80%) is further observed, since it also depends on the additional contribution of dampers that, if positioned at the same distance from the corners with respect the base setup, are subjected to larger uplifts as *B* increases, and so provide a greater contribution in terms of strength and stiffness.
- Effect of *H*. A small increment of all parameters is observed by increasing *H*, since it does not affect the deformation of the PT-bar and the uplifts to which axial dampers are subjected.
- Effect of $PT\text{-}Force_{in}$. An increase of $PT\text{-}Force_{in}$ of 34% and 51%, corresponds to an increase of F^* of 15% and 24% at the same value of drift (0.5%), respectively, due to the beneficial effect of the precompression in improving the strength and stiffness of the wall, also evident from the increase of 13% and 23% in terms of $F_{2\%}$ and stiffness *k* of 25% and 31%, respectively. No differences are observed in terms of $\Delta PT\text{-}Force_{2\%}$, since it is strictly related to the elongation of the PT-bar, which in turn is related to the drift from the geometrical considerations.
- Effect of *E*. An increase of *E* (25% and 45%), and proportionally of *G*, provides a small increase in terms of F^* (9% and 15%), $F_{2\%}$ (11% and 20%) and $\Delta PT\text{-}Force_{2\%}$ (7% and 13%), and, as expected, a strong effect on the increase of initial stiffness *k* of the Force/Drift curve (21% and 37%).
- Effect of Axial Dampers. The increase of the number of axial dampers (50% and 75%), leads to an increase of strength more evident in the value of F^* (31% and 56%) than $F_{2\%}$ (13% and 31%), since, in the second branch of the Force/Drift curve, they work in the

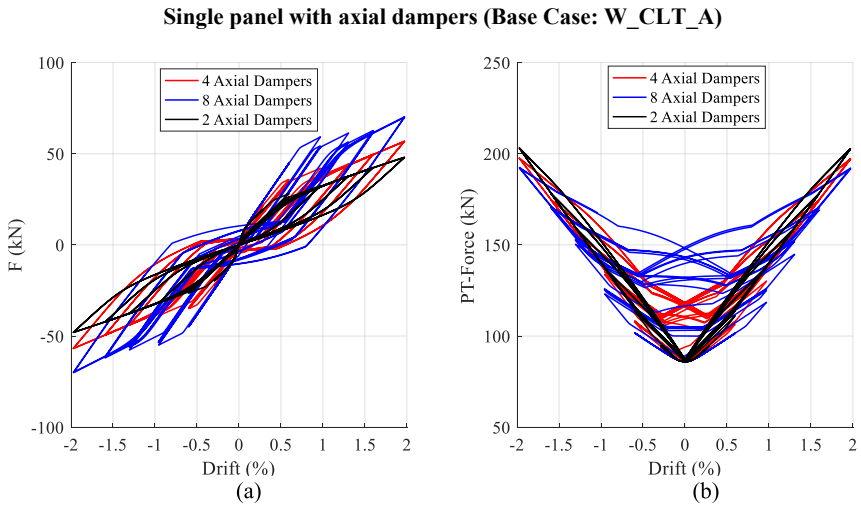


Fig. 18. Effect of the number of axial dampers on Force/Drift (a) and PT-Force/Drift curves (b) for single wall setups.

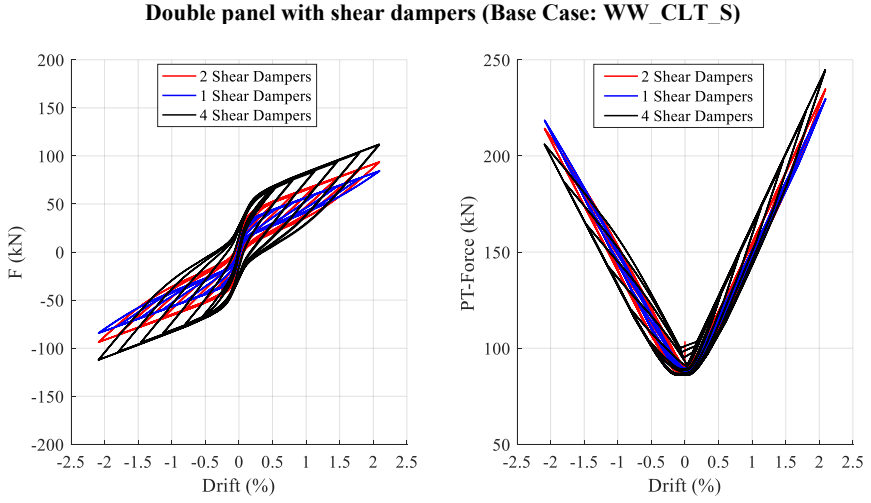


Fig. 19. Effect of the number of shear dampers on Force/Drift (a) and PT-Force/Drift curves (b) for double wall setups.

plastic field, so their contribution in terms of strength reduces. Further, the stiffness contribution of the axial dampers is also evident on the global Force/Drift curve in terms of k, which increases of 33% and 47%, respectively. Negligible effects can be observed on $\Delta PT\text{-}Force_{2\%}$, since it is strictly related to geometrical issues.

- Effect of Shear Dampers. The increase of the number of shear dampers (50% and 75%) provides similar effects of axial dampers in terms of increment of F^* (18% and 42%), $F_{2\%}$ (10% and 24%), and $\Delta PT\text{-}Force_{2\%}$ (6% and 10%). Contrarily, a reduction of k (−25% and −33%) is observed due to the presence of a smoothed pinching effect that influences the slope of the first branch of the Force/Drift curve.

In summary, the role of the different parameters on the global behaviour of the systems can be summarized as follow:

- as the base of the wall B increase, also initial stiffness, strength, PT-Force variation and dissipative capacity (if axial dampers are present) significantly increase;
- as the height of the wall H increase, the initial stiffness, strength and PT-Force change present a slight variation;
- as the initial PT-Force on the bar $PT\text{-}Force_{in}$ increases, also strength and stiffness increase, but the most important effect is connected to the re-centering capacity of the system that is significantly improved;
- as the number of axial dampers increases, also strength and dissipative capacity increase to the detriment of the re-centering capacity, which decreases;
- as the number of shear dampers increases, strength and dissipative capacity also increase, while the re-centering capacity shows only limited variations.

Table 4
Effect of different parameters (B, H, PT-Force$_{in}$, number of axial and shear dampers) on the response of single and double wall setups.

Single panel with axial dampers (Base Case: W_CLT_A)				
B (cm)	F* (kN)	$F_{2\%}$ (kN)	PT-Force$_{2\%}$ (kN)	k (kN/m)
100	**35**	**55**	**109**	**2000**
150	55	120	181	5000
200	75	170	236	10000
H (cm)	F* (kN)	$F_{2\%}$ (kN)	PT-Force$_{2\%}$ (kN)	k (kN/m)
300	**35**	**55**	**109**	**2000**
350	36	62	115	2098
400	37	65	119	2167
PT-Force$_{in}$ (kN)	F* (kN)	$F_{2\%}$ (kN)	PT-Force$_{2\%}$ (kN)	k (kN/m)
89	**35**	**55**	**109**	**2000**
135	41	63	107	2667
180	46	71	107	2917
Timber Characteristics (MPa)	F* (kN)	$F_{2\%}$ (kN)	PT-Force$_{2\%}$ (kN)	k (kN/m)
E=6000; G= 348	**32**	**49**	**197**	**2133**
E = 8000; G = 464	35	55	212	2713
E = 11000; G = 638	37.5	61.25	226	3378
Axial Dampers	F* (kN)	$F_{2\%}$ (kN)	PT-Force$_{2\%}$ (kN)	k (kN/m)
2	24	48	114	1333
4	**35**	**55**	**109**	**2000**
8	54	70	103	2500
Double panel with shear dampers (Base Case: WW_CLT_S)				
Shear Dampers	F* (kN)	$F_{2\%}$ (kN)	PT-Force$_{2\%}$ (kN)	k (kN/m)
1	33	85	117	6667
2	**40**	**94**	**125**	**5333**
4	57	112	130	5000

Therefore, in order to have a re-centering system characterized by a good dissipative capacity, it is important to provide an adequate number of dampers in the function of the initial *PT-Force$_{in}$* of the bars. Furthermore, without changing the number of dampers and *PT-Force$_{in}$*, it is possible to intervene in the strength and stiffness of the system by increasing the size of the walls.

6. Conclusions

The paper presents an advanced Finite Element nonlinear numerical model, developed in the OpenSEES framework, for the prediction of the cyclic response of Post-Tensioned dissipative timber walls systems. The proposed numerical model specifically accounts for both geometrical and mechanical non-linearities, the former related to the rocking behaviour of the system, the latter due to the hysteretic contribution of the dampers, which numerical force/displacement responses have been calibrated on experimental responses of the individual devices. The numerical model has been validated with different experimental campaigns, characterized by different wall subassemblies (single wall, single wall equipped with boundary columns, double walls), different materials (Laminated Veneer Lumber and Cross Laminated Timber), different number of PT-bar in each wall, different PT-Force applied to the walls, and different pattern of dampers (axial dampers, shear dampers or both). In particular, the comparisons between the global Force/Drift and PT-bar/Drift behaviour of the numerical and experimental response show a good agreement in terms of stiffness, strength, cyclic behaviour, and energy dissipation. Further, the numerical model can also provide local information often unavailable from experimental campaigns, such as the base deformation at each drift level, strictly related to the neutral axis depth or the force/displacement responses of dampers. The proposed numerical model proves to have general validity since it is able to capture the behaviour of different experimental campaigns, therefore, it can be used as an effective tool for modelling any further PT-wall system or for optimizing the design of PT-wall systems with its dampers in terms of energy dissipation for fixed values of drift.

A parametric analysis has been performed in order to evaluate the effect of some parameters, like as the wall base *B*, the wall height *H*, the initial post-tensioned force *PT-Force$_{in}$* of the bars, the timber characteristics in terms of elastic modulus *E*, the number of Axial Dampers and the number of Shear Dampers, on the global behavior of post-tensioned timber walls. The results show that the most significant increase of initial stiffness, strength, and PT-Force variation are due to the increase of the base wall *B*, while an increase of the initial bar *PT-Force$_{in}$* has an important effect on the re-centering capacity of the system; finally, the number of dampers greatly influence the dissipative capacity.

Further developments could be to employ the presented model in a more complex framework, together with the timber frame structure designed for gravity loads.

Author statement

Valentina Tomei: Conceptualization; Methodology; Software; Investigation; Data Curation; Writing - Original Draft; Writing - Review & Editing; Visualization. Maria Zucconi: Conceptualization; Methodology; Writing - Original Draft; Writing - Review & Editing;

Supervision. Barbara Ferracuti: Conceptualization; Methodology; Writing - Original Draft; Writing - Review & Editing; Supervision; Funding acquisition.

Declaration of competing interest

The authors declare that they have no known competing financial interests or personal relationships that could have appeared to influence the work reported in this paper.

Data availability

Data will be made available on request.

Acknowledgement

The financial support of ENHANCE 2021-2023 - Research Groups 2020 financed by the POR FESR Lazio 2014 - 2020 (Action 1.2.1)

References

[1] M. Fragiacomo, B. Dujic, I. Sustersic, Elastic and ductile design of multi-storey crosslam massive wooden buildings under seismic actions, Eng. Struct. (2011), https://doi.org/10.1016/j.engstruct.2011.05.020.
[2] I. Gavric, M. Fragiacomo, A. Ceccotti, Cyclic behavior of CLT wall systems: experimental tests and analytical prediction models, J. Struct. Eng. 141 (2015), https://doi.org/10.1061/(ASCE)ST.1943-541X.0001246.
[3] I. Sustersic, M. Fragiacomo, B. Dujic, Seismic analysis of cross-laminated multistory timber buildings using code-prescribed methods: influence of panel size, connection ductility, and schematization, J. Struct. Eng. (2016), https://doi.org/10.1061/(ASCE)ST.1943-541X.0001344.
[4] F. Asdrubali, B. Ferracuti, L. Lombardi, C. Guattari, L. Evangelisti, G. Grazieschi, A review of structural, thermo-physical, acoustical, and environmental properties of wooden materials for building applications, Build. Environ. (2017) 307–332, https://doi.org/10.1016/j.buildenv.2016.12.033.
[5] A. Sandoli, V. Tomei, B. Ferracuti, M. Zucconi, Challenges on Clt Structures Seismic Response: Traditional vs Low-Damage Systems, Eur. Conf. Earthq. Eng., Thessaloniki, 2018, p. 16th.
[6] L. Pozza, B. Ferracuti, M. Massari, M. Savoia, Axial – shear interaction on CLT hold-down connections – experimental investigation, Eng. Struct. 160 (2018) 95–110, https://doi.org/10.1016/j.engstruct.2018.01.021.
[7] J. Liu, F. Lam, R.O. Foschi, M. Li, Modeling the coupling effect of CLT connections under biaxial loading, J. Struct. Eng. (2020), https://doi.org/10.1061/(asce)st.1943-541x.0002589.
[8] J. Liu, F. Lam, Experimental test of coupling effect on CLT hold-down connections, Eng. Struct. (2019), https://doi.org/10.1016/j.engstruct.2018.10.063.
[9] A. Iqbal, S. Pampanin, A. Palermo, A.H. Buchanan, Performance and design of LVL walls coupled with UFP dissipaters, J. Earthq. Eng. (2015), https://doi.org/10.1080/13632469.2014.987406.
[10] F. Sarti, A. Palermo, S. Pampanin, Quasi-static cyclic testing of two-thirds scale unbonded posttensioned rocking dissipative timber walls, J. Struct. Eng. (2016), https://doi.org/10.1061/(ASCE)ST.1943-541X.0001291.
[11] A. Hashemi, P. Quenneville, Large-scale testing of low damage rocking Cross Laminated Timber (CLT) wall panels with friction dampers, Eng. Struct. 206 (2020), 110166, https://doi.org/10.1016/j.engstruct.2020.110166.
[12] W.C. Stone, G.S. Cheok, J.F. Stanton, Performance of hybrid moment-resisting precast beam-column concrete connections subjected to cyclic loading, ACI Struct. J. (1995), https://doi.org/10.14359/1145.
[13] M.J.N. Priestley, S.S. Sritharan, J.R. Conley, S. Pampanin, Preliminary results and conclusions from the PRESSS five-story precast concrete test building, PCI J. (1999), https://doi.org/10.15554/pcij.11011999.42.67.
[14] C. Christopoulos, A. Filiatrault, C.M. Uang, B. Folz, Posttensioned energy dissipating connections for moment-resisting steel frames, J. Struct. Eng. (2002), https://doi.org/10.1061/(asce)0733-9445(2002)128:9(1111).
[15] D. Marriott, S. Pampanin, D. Bull, A. Palermo, Dynamic testing of precast, post-tensioned rocking wall systems with alternative dissipating solutions, Bull. New Zeal. Soc. Earthq. Eng. (2008), https://doi.org/10.5459/bnzsee.41.2.90-103.
[16] T. Smith, S. Pampanin, A. Buchanan, M. Fragiacomo, Feasibility and Detailing of Post-tensioned Timber Buildings for Seismic Areas, NZSEE Conf., 2008, 2008.
[17] A. Kramer, A.R. Barbosa, A. Sinha, Performance of steel energy dissipators connected to cross-laminated timber wall panels subjected to tension and cyclic loading, J. Struct. Eng. (2016), https://doi.org/10.1061/(ASCE)ST.1943-541X.0001410.
[18] F. Sarti, A. Palermo, S. Pampanin, Fuse-type external replaceable dissipaters: experimental program and numerical modeling, J. Struct. Eng. (2016), https://doi.org/10.1061/(ASCE)ST.1943-541X.0001606.
[19] R. Scotta, L. Marchi, D. Trutalli, L. Pozza, A dissipative connector for CLT buildings: concept, design and testing, Materials (2016), https://doi.org/10.3390/ma9030139.
[20] J.M. Kelly, R.I. Skinner, A.J. Heine, Mechanisms of energy absorption in special devices for use in earthquake resistant structures, Bull. New Zeal. Soc. Earthq. Eng. 5 (3) (1972) 63–88.
[21] R.I. Skinner, J.M. Kelly, A.J. Heine, Hysteretic Dampers for Earthquake-resistant Structures, Earthq. Eng. Struct. Dyn., 1974, https://doi.org/10.1002/eqe.4290030307.
[22] A. Baird, T. Smith, A. Palermo, S. Pampanin, Experimental and Numerical Study of U-Shape Flexural Plate (UFP) Dissipators, NZSEE Conf, 2014.
[23] A. Tatar, D.M. Dowden, Analytical and numerical investigation of a low-damage uplift friction damper for self-centering cross-laminated timber rocking walls, Eng. Struct. 254 (2022), 113836, https://doi.org/10.1016/j.engstruct.2021.113836.
[24] R. Ganey, J. Berman, T. Akbas, S. Loftus, J. Daniel Dolan, R. Sause, J. Ricles, S. Pei, J. Van De Lindt, H.E. Blomgren, Experimental investigation of self-centering cross-laminated timber walls, J. Struct. Eng. (2017), https://doi.org/10.1061/(ASCE)ST.1943-541X.0001877.
[25] M. Massari, M. Savoia, A.R. Barbosa, Experimental and numerical study of two-story post-tensioned seismic resisting CLT wall with external hysteretic energy dissipaters, in: Atti Del XVII Convegno ANIDIS L'ingegneria Sismica Ital., 2017.
[26] Z. Chen, M. Popovski, A. Iqbal, Structural performance of post-tensioned CLT shear walls with energy dissipators, J. Struct. Eng. 146 (2020), https://doi.org/10.1061/(asce)st.1943-541x.0002569.
[27] R. Henry, S. Aaleti, S. Sritharan, J. Ingham, Seismic analysis of a low-damage precast wall with end columns (PreWEC) including interaction with floor diaphragms, Struct. Eng. Soc. New Zeal. 25 (1) (2012) 69–81.
[28] F. Sarti, A. Palermo, S. Pampanin, Development and testing of an alternative dissipative posttensioned rocking timber wall with boundary columns, J. Struct. Eng. (2016), https://doi.org/10.1061/(ASCE)ST.1943-541X.0001390.
[29] L. Pozza, L. Benedetti, V. Tomei, B. Ferracuti, M. Zucconi, C. Mazzotti, Cyclic response of CLT post-tensioned walls: experimental and numerical investigation, Construct. Build. Mater. 308 (2021), 125019, https://doi.org/10.1016/J.CONBUILDMAT.2021.125019.
[30] F. Sarti, Seismic Design of Low Damage Post-Tensioned Timber Wall Systems, University of Canterbury Christchurch, New Zealand, 2015.
[31] L. Pozza, L. Benedetti, V. Tomei, B. Ferracuti, M. Zucconi, C. Mazzotti, Post-Tensioned low damage CLT walls with replaceable hysteretic devices – concept, experimental and numerical characterization, in: M. Papadrakakis, M. Fragiadakis (Eds.), 8th Int. Conf. Comput. Methods Struct. Dyn. Earthq. Eng. Streamed

from Athens, Greece 28-30 June 2021, Institute of Structural Analysis and Antiseismic Research School of Civil Engineering National Technical University of Athens (NTUA) Greece, Greece, 2021, pp. 2352–2358. Streamed from Athens.
[32] D. Moroder, T. Smith, A. Dunbar, S. Pampanin, A. Buchanan, Seismic testing of post-tensioned Pres-Lam core walls using cross laminated timber, Eng. Struct. 167 (2018) 639–654, https://doi.org/10.1016/j.engstruct.2018.02.075.
[33] S. Pei, J.W. Van De Lindt, A.R. Barbosa, J.W. Berman, E. McDonnell, J. Daniel Dolan, H.E. Blomgren, R.B. Zimmerman, D. Huang, S. Wichman, Experimental Seismic Response of a Resilient 2-Story Mass-Timber Building with Post-Tensioned Rocking Walls, J. Struct. Eng. (United States), 2019, https://doi.org/10.1061/(ASCE)ST.1943-541X.0002382.
[34] T.X. Ho, T.N. Dao, S. Aaleti, J.W. van de Lindt, D.R. Rammer, Hybrid system of unbonded post-tensioned CLT panels and light-frame wood shear walls, J. Struct. Eng. 143 (2017), 04016171, https://doi.org/10.1061/(asce)st.1943-541x.0001665.
[35] J.R. Brown, M. li, A. Palermo, S. Pampanin, F. Sarti, Nokes Roger, Experimental testing and analytical modelling of single and double post-tensioned CLT shear walls, Eng. Struct. 256 (2022), https://doi.org/10.1016/j.engstruct.2022.114065.
[36] A. Polastri, D. Casagrande, Mechanical behaviour of multi-panel cross laminated timber shear-walls with stiff connectors, Construct. Build. Mater. 332 (2022), 127275, https://doi.org/10.1016/j.conbuildmat.2022.127275.
[37] R. Thiers-Moggia, C. Málaga-Chuquitaype, Performance-based seismic design and assessment of rocking timber buildings equipped with inerters, Eng. Struct. 248 (2021), 113164, https://doi.org/10.1016/j.engstruct.2021.113164.
[38] Y. Lu, Q. Lv, Y. Liu, Experimental and numerical study on seismic performance of CLB rocking wall with bending-friction coupled dampers, J. Build. Eng. 45 (2022), 103622, https://doi.org/10.1016/j.jobe.2021.103622.
[39] X. Sun, M. He, Z. Li, F. Lam, Seismic performance assessment of conventional CLT shear wall structures and post-tensioned CLT shear wall structures, Eng. Struct. 196 (2019), 109285, https://doi.org/10.1016/j.engstruct.2019.109285.
[40] X. Sun, M. He, Z. Li, F. Lam, Seismic performance of energy-dissipating post-tensioned CLT shear wall structures I: shear wall modeling and design procedure, Soil Dynam. Earthq. Eng. 131 (2020), https://doi.org/10.1016/j.soildyn.2019.106022.
[41] X. Sun, M. He, Z. Li, F. Lam, Seismic performance of energy-dissipating post-tensioned CLT shear wall structures II: dynamic analysis and dissipater comparison, Soil Dynam. Earthq. Eng. 130 (2020), https://doi.org/10.1016/j.soildyn.2019.105980.
[42] D.S. Pilon, A. Palermo, F. Sarti, A. Salenikovich, Benefits of multiple rocking segments for CLT and LVL Pres-Lam wall systems, Soil Dynam. Earthq. Eng. 117 (2019) 234–244, https://doi.org/10.1016/j.soildyn.2018.11.026.
[43] H. Hasani, K.L. Ryan, Effect of partition walls on the seismic response of mass-timber buildings with a post-tensioned rocking wall system, Eng. Struct. 262 (2022), 114316, https://doi.org/10.1016/J.ENGSTRUCT.2022.114316.
[44] D. Huang, S. Pei, A. Busch, Optimizing displacement-based seismic design of mass timber rocking walls using genetic algorithm, Eng. Struct. 229 (2021), 111603, https://doi.org/10.1016/j.engstruct.2020.111603.
[45] STIC, Design Guide Australia and New Zealand – Post-tensioned Timber Buildings, 2013.
[46] A.W. Wilson, C.J. Motter, A.R. Phillips, J.D. Dolan, Modeling techniques for post-tensioned cross-laminated timber rocking walls, Eng. Struct. 195 (2019) 299–308, https://doi.org/10.1016/j.engstruct.2019.06.011.
[47] V. Tomei, M. Zucconi, B. Ferracuti, Post-Tensioned low damage timber walls with dissipative devices, in: M. Papadrakakis, M. Fragiadakis (Eds.), 8th Int. Conf. Comput. Methods Struct. Dyn. Earthq. Eng. Streamed from Athens, Greece 28-30 June 2021, Institute of Structural Analysis and Antiseismic Research School of Civil Engineering National Technical University of Athens (NTUA) Greece, Greece, 2021, pp. 2314–2322. Streamed from Athens.
[48] S. Mazzoni, F. McKenna, M.H. Scott, G.L. Fenves, OpenSees command language manual, Pacific Earthq. Eng. Res. Cent. 2 (2006) 1–465.
[49] S.R. Ganey, Seismic Design and Testing of Rocking Cross Laminated Timber Walls, Master Thesis, University of Washington, 2015.
[50] I. Computers Structures, CSI Analysis Reference Manual: for SAP2000, ETABS, SAFE and CSIBridge., (210AD).
[51] Z. Chen, M. Popovski, Material-based models for post-tensioned shear wall system with energy dissipators, Eng. Struct. 213 (2020), https://doi.org/10.1016/j.engstruct.2020.110543.
[52] Dassault Systèmes Simulia Corp, ABAQUS Analysis User's Manual, 2016, Version 6.14.
[53] F. McKenna, M.H. Scott, G.L. Fenves, Nonlinear finite-element analysis software architecture using object composition, J. Comput. Civ. Eng. (2010), https://doi.org/10.1061/(ASCE)CP.1943-5487.0000002.
[54] F.E. Fllippou, E.P. Popov, V. V Bertero, Effects of Bond Deterioration on Hysteretic Behavior of Reinforced Concrete Joints, Report EERC 83-19, Earthquake Engineering Research Center, University of California, Berkeley, 1983.
[55] W. Ramberg, W.R. Osgood, Description of Stress-Strain Curves by Three Parameters, Technical Note No. 902, National Advisory Committee For Aeronautics, Washington DC, 1943.